BUCKLING OF MULTILAYERED METAL COMPOSITE DOMES

J. Blachut, P. Smith
The University of Liverpool, Mechanical Engineering
Liverpool L69 3GH
U.K.

ABSTRACT

Results of a numerical and experimental investigation into static stability of externally pressurised hemispherical and torispherical domes are provided in this paper. Hybrid wall of considered domes includes steel-aluminium, steel-aluminium-steel and copper-steel-copper configurations.
Buckling/collapse tests were conducted on domes manufactured from copper-steel-copper layered material. Details are provided of manufacture of domes, pre-test measurements, testing, and the FE analysis of measured geometries of domes. Five pairs of laboratory scale domes were tested. Each pair had nominally identical geometry. Total wall thickness of copper-steel-copper domes was about 1.1 mm. Inner and outer layers were copper, each 0.05 mm thick. Both types of heads, i.e., hemispherical and torispherical were manufactured from flat sheets using spinning. The (radius-to-wall-thickness)-ratio, R/t, was in the range from 40 to 200. Two values of the (knuckle-radius-to-diameter)-ratio in torispheres were used, i.e., 10% and 17%. Single, quasi-static incremental loading was applied in all cases. The end of load carrying capacity was sudden and well defined. Values of experimental buckling pressures varied from 1.7 MPa to 10 MPa.

1. INTRODUCTION

Layered structures are extensively used in as diverse applications as in aircrafts, thin film deposition in semiconductor devices, heat exchangers, etc. Such structures are subjected to a variety of loading types with some of them being capable of causing buckling. One particular sub-set of layered structures contained multilayered metal composite plates and shells, where early studies showed that buckling could be triggered by thermal loading. Thermally induced elastic buckling of layered shells has recently been studied for bimetallic hemispheres and multilayer circular panels, [1, 2]. References to the past work on buckling of bimetal components can be found in papers [1, 2]. Reference [1] provides details about a wider study into the elastic buckling behaviour of circular panels for combination of temperature, external pressure and edge loading. Loss of local stability in a cracked bimetal plate was studied in [3]. Other known work in this area includes analytical study into residual stresses caused by manufacturing in two-, and in three-layered plates, [4].
Developments in manufacturing of metal composites have increased interests in their structural performance. Rolling and diffusion welding, for example, can successfully be used to manufacture composite multilayer materials. Aluminium, copper, molybdenum, steel and titanium have been used in the past in layered metal composites (primarily in plates). The literature review indicates that there are no known data on static stability analysis/tests of multilayered metallic, doubly curved shells. Structure of multilayered metal wall in shells can be tailored to specific needs despite the fact that properties of individual layers remain isotropic. For example, multilayered vessels constructed of metallic layers can be used in corrosive environment where a core layer of material can provide the majority of load bearing, and an external/internal layer is used to resist corrosion. Heat exchangers are commonly composed of titanium and steel since it would be cost prohibitive to construct the heat exchanger entirely of titanium. Other physical properties of individual layers can also be utilized. Reflectivity of copper is 25 % higher than that of aluminium. Melting temperature of copper is 60 % higher than that of aluminium. Also, it is known that some of the most dangerous bacteria are being killed when in contact with copper. Comparable magnitude of coefficient of thermal expansion of steel and copper is another useful match of properties. These and other properties could offer designers more choices.
Structural integrity of externally pressurised domed ends onto cylindrical shells, and made either from steel or CFRP/GFRP material, has been extensively studied in the past. Static and dynamic buckling of these shells are two possible modes of failure due to external pressure. References [4 – 8] provide more recent updates on structural integrity of externally pressurised domed closures. Despite of the accumulated knowledge on buckling resistance of domed end closures there are still a number of issues related to reliable prediction of their load carrying capacity. Whilst research into their structural performance continues, design codes [9 – 11], are still used for practical applications. Some geometries are not covered in the current design codes, e.g., prolate elliptical domes, and results of an experimental and numerical study into their buckling resistance can be found in Ref. [12].

The current paper aims to assess static stability of externally pressurised multilayered metal composite hemispherical and torispherical domes. This is a numerical and experimental work.

2. BACKGROUND AND MODELLING DETAILS

Typical geometry of domed ends includes hemispherical or torispherical shapes. Their shapes are sketched in Fig. 1. Assume that both types of domes have a short cylindrical portion of length, L, attached to them, with both shells having the same, uniform wall thickness, t. It is customary to describe geometry of a torispherical shell by the (D/t)-, (R_s/D)-, and (r/D)-ratios. In the current paper these ratios are referred to the shell mid-surface. When a dome is subjected to incremental pressure loading it can suddenly lose its stability either through asymmetric bifurcation or axisymmetric collapse. Both of these modes can be either elastic or elastic-plastic. As an illustration, consider a torispherical head with its geometry given by the diameter-to-thickness ratio, D/t = 1000, the knuckle

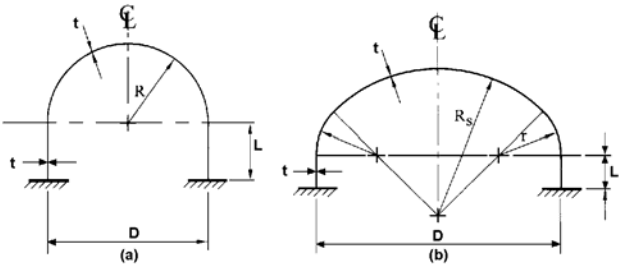

FIG. 1 Geometry of hemispherical (Fig. 1a) and torispherical (Fig. 1b) end closures.

radius-to-diameter ratio, r/D = 0.10, the spherical-radius-to-diameter ratio, R_s/D = 1.0, and subjected to uniform external pressure p. Let the torisphere be manufactured from a single layer of steel for which material properties are given in Table 1. Assume that there is no cylindrical flange, i.e., L ≡ 0.0, and the dome is fully clamped at its edge.

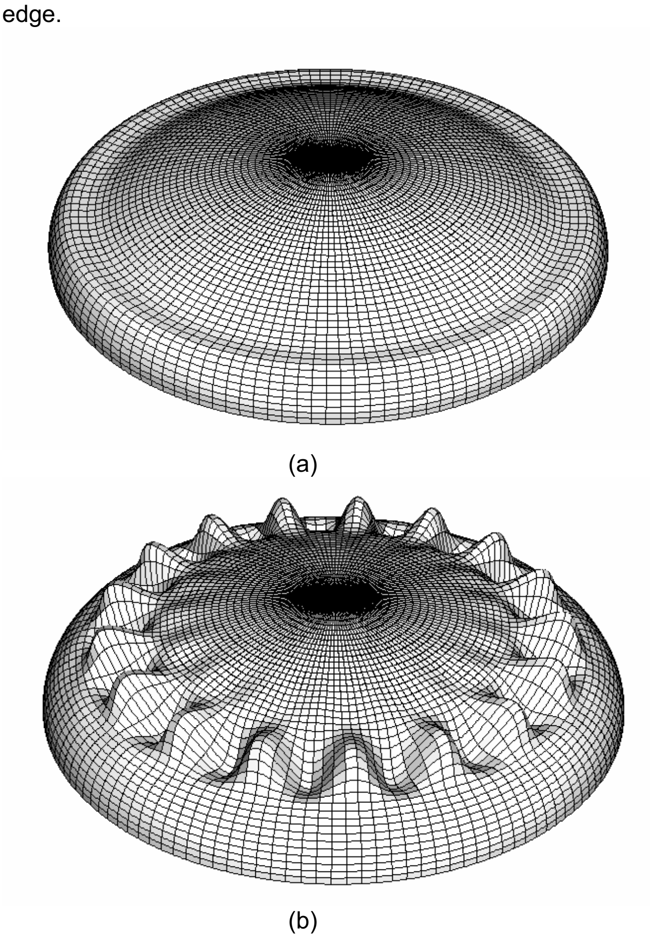

FIG. 2 Deformed shape of torispherical shell just prior to buckling (Fig. 2a) and its shape at bifurcation buckling (Fig. 2b).

Pre-buckling shape of externally pressurised torisphere with the diameter-to-thickness, (D/t)-ratio 1000, is shown in Fig. 2a. This shell is able to support external pressure for up to a certain magnitude at which the axisymmetric deformation, seen in Fig. 2a, suddenly changes its shape. This pressure, corresponding to an eigenvalue, is also known as bifurcation pressure. Its magnitude in the current case is, p_{bif} = 0.126 MPa. Fig. 2b depicts

	E (GPa)	σ_{yp} (MPa)	υ
Aluminium	70.0	300.0	0.3
Copper	120.0	70.0	0.3
Steel	210.0	350.0	0.3
C-S-C(1)	213 - 239	310 - 315	0.3
C-S-C(2)	183.1	237.9	0.327

TAB 1. Material data for aluminium, copper, and steel layers. C-S-C ≡ Copper-Steel-Copper three layer material. C-S-C(1) ≡ average material properties obtained from tests; C-S-C(2) ≡ material properties quoted by manufacturer.

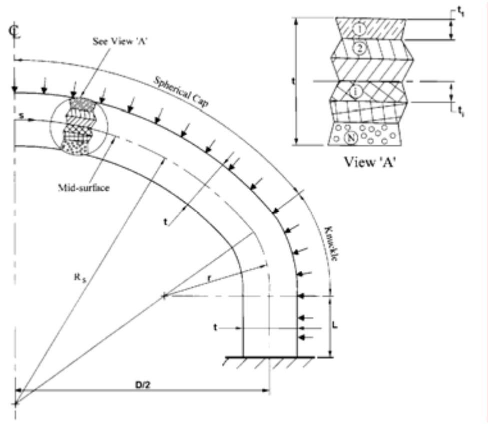

FIG. 3 Illustration of N-layer torispherical shell subjected to uniform external pressure. Each layer is made from a different metal. Note: Shell geometry is defined using its mid-surface.

eigenshape, i.e. the shape at pressure equal to bifurcation, and which has n = 17 circumferential waves. The influence of the (D/t)-, (R_s/D)-, and (r/D)-ratios on buckling performance of steel torispheres was addressed in Ref. [13], where results of a wide parametric study are provided. Buckling/strength performance of multi-layer domes made from Carbon Fibre Reinforced Plastics, and subjected to external pressure was investigated in Refs [14 – 16]. Filament winding and draping of pre-preg woven fabric were used in manufacturing of hemispherical and torispherical shells.

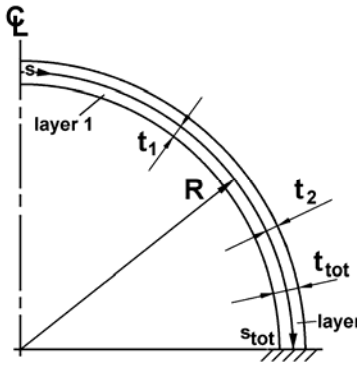

FIG. 4 Two-layer hemispherical shell subjected to external pressure.

The current paper concentrates on domes made from layered metallic material. As an illustration, consider a torispherical dome made from N different layers, diameter, D, constant and uniform wall thickness, t, fully clamped at

the end of cylindrical flange of length, L, and subjected to uniform external pressure, p, as illustrated in Fig. 3. Let us assume that layer number, i, has elastic constants [E_i, υ_i], thickness, t_i, and the yield point of material σ^i_{yp}. Table 1 contains typical values for aluminium, copper and steel which were adopted in numerical calculations. Material properties of each layer are to be modelled as elastic perfectly plastic. For strain-hardening material, e.g. aluminium alloys the yield point is to be based on 0.2 % proof stress. All numerical calculations in the current paper are based on the FE code ABAQUS [17], and finite difference code BOSOR5 [18].
Buckling performance of a 2-layer, steel-aluminium, hemisphere is examined first in the next section.

	t_{min} (mm)	t_{max} (mm)	t_{ave} (mm)	Stdev (mm)
S1	0.990	1.150	1.088	0.018
S2	1.040	1.130	1.086	0.015

TAB 2. Measured thickness of sheets S1 and S2.

3. TWO LAYER STEEL-ALUMINIUM HEMISPHERE

Consider the hemisphere of mid-surface radius, R, shown in Fig. 4. The dome is of total wall thickness, t_{tot}, and the wall is constructed from two layers of material with thicknesses, t_1, and t_2. In the case of Fig. 4 the thickness of the two layers is equal. The dome is fully clamped at the base, and it is subjected to uniform external pressure. The two materials chosen for this section are: mild steel and aluminium. Material properties of both layers are designated here as [E_s, σ_{yps}, v_s], and [E_a, σ_{ypa}, v_a] for steel and aluminium, respectively and they are given in Table 1.

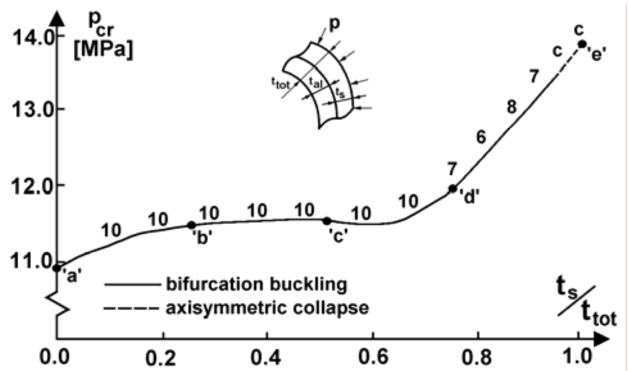

FIG. 5 Plot of buckling strength versus thickness of steel layer (t_s/t_{tot} ≡ 1.0 corresponds to steel only wall thickness). Numbers above the curve show number of waves in the eigenshape. Note: steel forms the outer layer.

Both materials were modelled as elastic-perfectly plastic. The total thickness of the dome was set to D/t_{tot} = 100 and the proportion of the shell wall occupied by each of the two layers was varied. This total thickness is sufficiently thick for plasticity to be present during pressurisation of the dome and, as such, the yield strengths of the two materials can take a part in the dome's failure. The other consideration to make is the 'layup' of the dome, i.e., 'steel

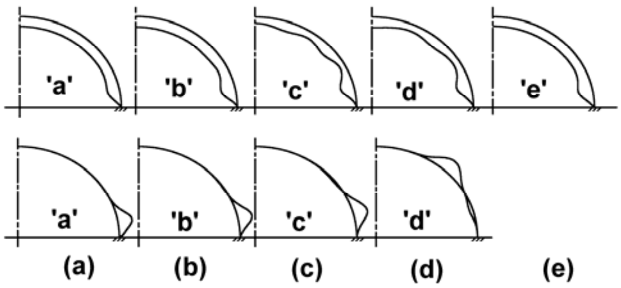

FIG. 6 Pre-buckling shapes, 'a', …, 'd', in the top row and the corresponding eigenshapes are plotted in the lower row. The case 'e' corresponds to axisymmetric collapse.

inside', or 'steel outside'. Firstly, steel outside was considered. The thickness of the outer steel layer was varied from t_s/t_{tot} = 0.0 to t_s/t_{tot} = 1.0. The failure pressures, as computed by BOSOR5, are shown in Fig. 5. It is seen that by introducing an outer layer of steel the failure pressure is only marginally increased. It is not until the thickness of the steel occupies over 60% of the shell wall that the failure pressure is increased, after which the failure pressure increases in an almost linear fashion until the dome is composed entirely of steel. Also given in Fig. 5 is the mode of failure, i.e., bifurcation buckling or axisymmetric collapse. Bifurcation is indicated by the number of circumferential waves, which is labelled next to the curve (c ≡ collapse). The number of circumferential waves at buckling is seen to decrease with increasing amount of steel, until the failure mode switches to collapse when the wall is composed of approximately 90% steel.

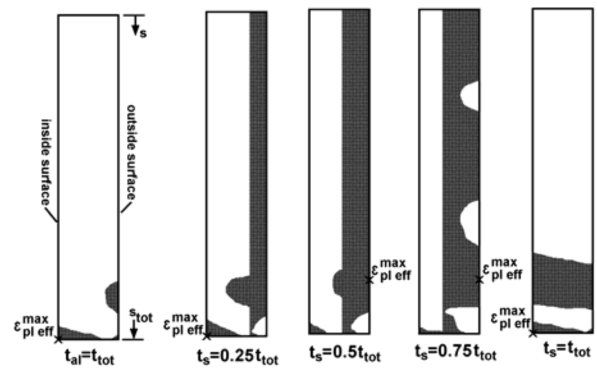

FIG. 7 Spread of plastic strain across the wall thickness, at the buckling/collapse pressure level, for five configurations, 'a', ….., 'e', marked in FIG. 5.

The buckling modes of five cases of the cases of t_s/t_{tot} = 0.00, 0.25, 0.50, 0.75 and 1.00 (labelled as 'a', 'b', 'c', 'd', 'e', in Fig. 5) are shown in Fig. 6 where the buckling mode for 'd' was seen to shift up the meridian. Case 'e' failed by collapse. To further investigate the spread of plasticity throughout a two layered dome, plots of plasticity in the shell wall, just prior to failure, were produced for the cases 'a', 'b', 'c', 'd', 'e'. The plots are shown in Fig. 7 where it is seen that the steel outer layer is almost entirely plastic just prior to failure while the aluminium layer is able to remain largely elastic. In addition, the location, and magnitude, of the maximum plastic strains in the shell wall just prior to failure have been plotted. It is seen that for cases, 'c' and 'd' the maximum plastic strain occurs away from the base of the dome, on the outside surface. For the other three

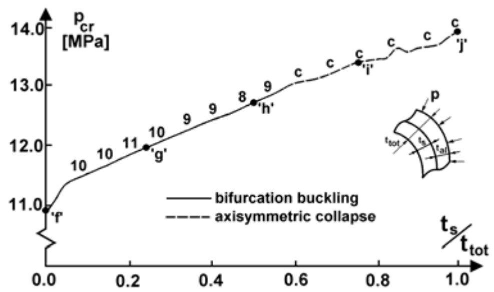

FIG. 8 Plot of buckling strength versus thickness of steel layer (t_s/t_{tot} ≡ 1.0 corresponds to steel only wall thickness). Numbers above the curve show number of waves in the eigenshape. Note: aluminium forms the outer layer.

cases the maximum plastic strain occurs at the base, on the inside surface. The layup of the dome was then reversed meaning the steel layer was on the inside of the shell. The difference this makes on the failure pressure of the dome is shown in Fig. 8 where the transition from an

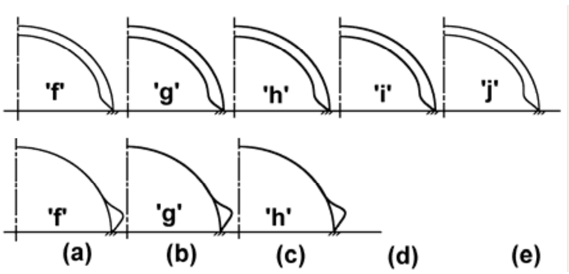

FIG. 9 Pre-buckling shapes 'f', 'g', and 'h' in the upper row, and the corresponding eigenshapes at the lower row. Shapes at collapse at points 'i', and 'j'. All points refer to FIG. 8.

aluminium dome to a steel dome is almost linear. Note also how the mode of failure is changing from bifurcation buckling with 10 waves, to axisymmetric collapse as the thickness of the steel layer is increased. Buckling modes of five cases labelled 'f', 'g', 'h', 'i', 'j' in Fig. 8 are shown in Fig. 9 where the three cases which buckled ('f', 'g', 'h') did so near the base of the dome. As was the case for steel outside, the spread of plasticity just prior to failure for five

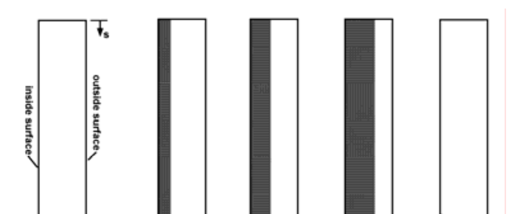

FIG. 10 Spread of plastic strains just prior to bifurcation/collapse for aluminium-steel hemisphere (see FIG. 8).

different configurations of dome was computed. The results are shown in Fig. 10 where again, the steel layer is almost entirely plastic while the aluminium layer is able to remain largely elastic during pressurisation. Also shown in

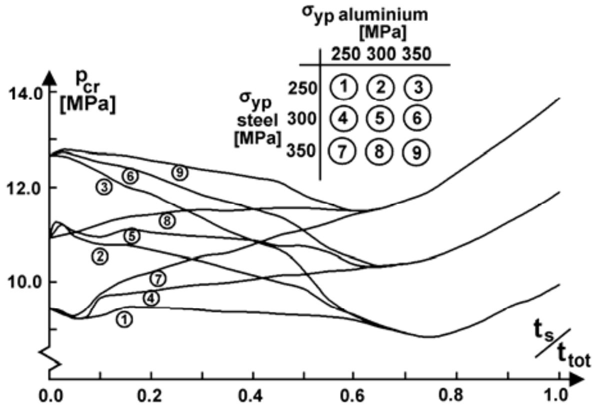

FIG. 11 Plot of failure load versus thickness of steel/aluminium layers for a range of yield magnitudes of steel and aluminium (with steel being the outer layer).

Fig. 10 is that the location of the maximum plastic strain in the shell wall just prior to failure occurs at the base, on the inside surface for all five cases 'f' – 'j'. To investigate the interaction of different yield strengths, the same procedure of varying the thickness of the steel layer in the shell wall was followed, using several combinations of yield for the two layers. The yield strengths used correspond to σ_{yp} = 250, 300 and 350 MPa. It is seen in Fig. 11 that for a steel outer layer the trend seen earlier in Fig. 5 remains the same, i.e., there is an increase in failure pressure after $t_s \approx 0.65t_{tot}$. What is also interesting to note after this point is that the failure pressure of the dome is independent of the yield strength of aluminium. Fig. 12 shows how for a steel inner layer the transition from steel to aluminium is nearly linear regardless of the combination of yield strengths

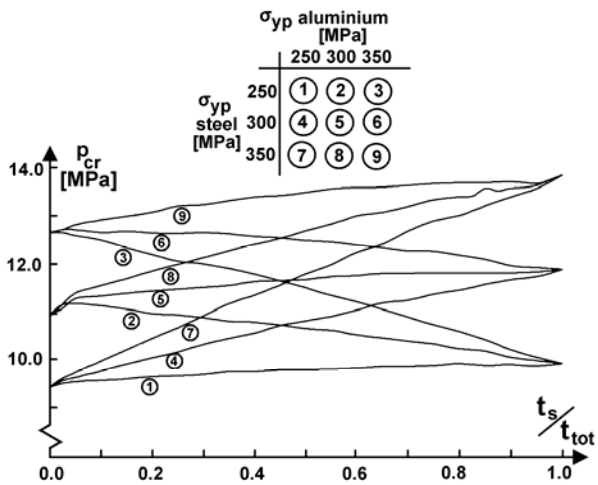

FIG. 12 Plot of failure load versus thickness of steel/aluminium layers for a range of yield magnitudes of steel and aluminium (with aluminium being the outer layer).

used. Furthermore, unlike in Fig. 11, none of the nine curves in Fig. 12 converge, i.e., the failure pressure of the dome is always dependent on the mechanical properties of both the constituent layers. Thus, the designer has a range of materials and thicknesses to choose from to achieve a required pressure resistance.

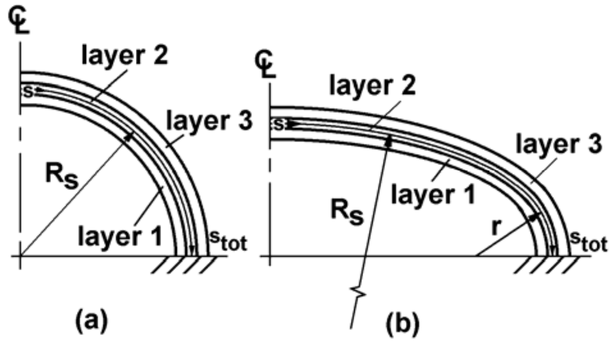

FIG. 13 Composition of the wall in three layered metallic domes: (a) hemisphere (Fig. 13 a) and torisphere (Fig. 13b).

4. THREE LAYER STEEL-ALUMINIUM-STEEL DOMES

The shell geometries considered for three layered shells were torispheres and hemispheres. The procedure was similar to that followed for two layered shells in that layer thicknesses were varied in order to asses the effect on pressure resistance. The material layup selected for investigation was copper-steel-copper, as this was the material configuration available for experimentation. Fig. 13 shows the geometries of shells and layers comprising the hemisphere and torisphere. All dimensions are measured to the middle surface of the total thickness and all layers are of constant thickness as one moves along the meridian. Analysis was made using BOSOR5. The material properties were selected from Table 1 and they

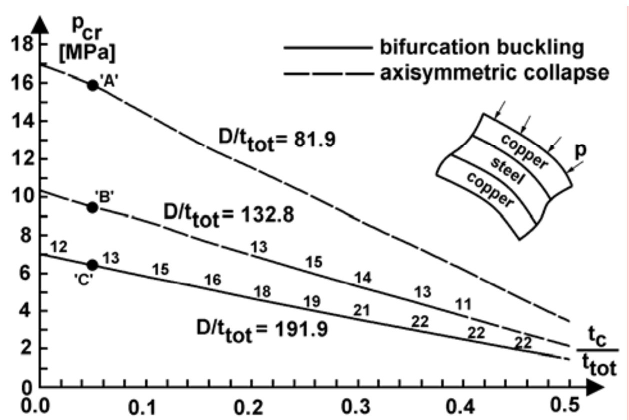

FIG. 14 Plot of failure pressures in copper-steel-copper domes versus thickness of copper layer in three hemispherical shells.

were modelled as elastic-perfectly plastic. The procedure was to start with a steel dome and add layers of copper of equal thickness on inside and outside surfaces. The thickness of the steel core is reduced in order to maintain the same total thickness. The thickness of the outer layers can therefore occupy from 0.0 to 0.5 of the total wall thickness, t_{tot}. Results for three configurations of hemispheres are shown in Fig. 14, where there is an almost linear transition from a steel dome (t_c/t_{tot} = 0.0) to a copper dome (t_c/t_{tot} = 0.5). Results for two torispherical geometries are shown in Fig. 15 where there is a non-linear transition from steel domes to copper domes. The

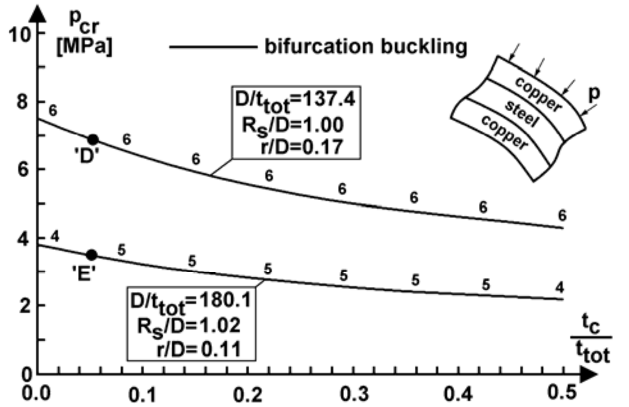

FIG. 15 Failure pressure for two configurations of copper-steel-copper torispheres. The thickness of the inner and outer layers of copper is varied. Total wall thickness remains constant.

five nominally manufactured configurations of test domes are labelled in Figs 14 and 15 as ‘A’, ‘B’, ‘C’, ‘D’, ‘E’. The plastic straining in domes A-E just prior to failure have been plotted in Fig. 16. It is seen that for hemispheres the maximum plastic straining occurs at the base of the dome, while for torispheres, the maximum plastic straining occurs at the junction between knuckle and crown. Note how the outer copper layers are being almost entirely plastically strained, and the internal steel layer can remain almost entirely elastic for all five cases.

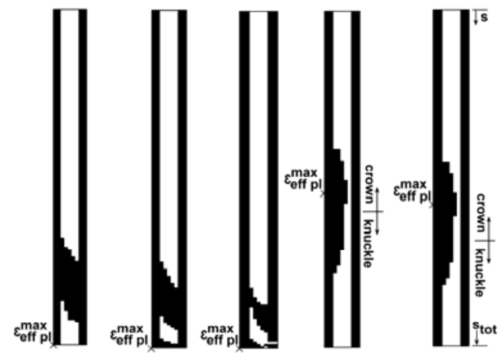

FIG. 16 Spread of plastic strains in copper-steel-copper domes corresponding to configurations ‘A’, ‘B’, ‘C’, ‘D’, and ‘E’ denoted in Figs 14 and 15. Maximum plastic straining at bifurcation/collapse loads corresponds to 2.37%, 2.58%, 1.76%, 0.85%, and 0.76%, respectively.

5. EXPERIMENTATION: THREE LAYER COPPER-STEEL-COPPER DOMES

5.1 Details of parent material

Experimentation was conducted on a three layered material, comprised of copper-steel-copper. The multilayer material was supplied as a flat sheet. Two sheets of hybrid material were labelled as S1 and S2. The dimensions of the sheets were 940mm × 500mm and 900 × 500mm. The nominal total thickness of the sheets quoted by manufacturer was 1.10 mm. The nominal thicknesses of the three layers was quoted as being: (i) copper 0.03 mm – 0.05 mm, (ii) steel 1.00 mm, and (iii) copper 0.03 mm –

0.05 mm. The sheets were measured for thickness on a 25mm grid giving 21 × 40 = 840 measuring points for S1 and 39 × 21 = 819 measuring points for S2. The minimum, maximum and average thicknesses along with standard deviation of the two sheets are summarised in Table 2. The largest difference in thickness was in sheet S1 where there was a 13.9% difference between t_{max} and t_{min}. This is due to the thickness at the edge of the sheets being quite changeable. As such, blanks cut for domes to be spun would avoid sheet edge material.

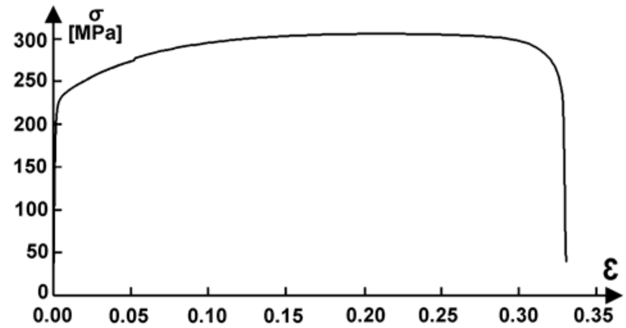

FIG. 17 Typical plot of uniaxial tension stress-strain curve obtained for a three layered copper-steel-copper flat coupon.

It was anticipated that the laminate would have anisotropic material properties. This is due to the two-stage hot rolling process used during manufacture of the laminate. Thus, it was decided to test the properties of the multilayer material in several directions in order to assess the level of anisotropy in the sheet. A number of coupons of 12.5mm width and 50mm gauge length were prepared in accordance with BS EN 10002:2001 [19], and were taken from sheet S1 in directions 0°, 90° and ± 45°. Some of coupons were strain gauged on both sides in both longitudinal and transverse directions (i.e., four strain gauges per coupon) to calculate Poisson's ratio.

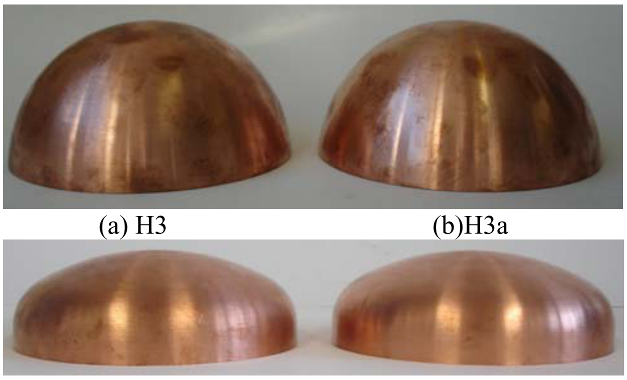

(a) H3 (b)H3a

(c) T2 (d) T2a

FIG. 18 View of two nominally identical three layer copper-steel-copper domes (hemispheres H3 and H3a, and two torispheres, T2 and T2a).

The coupons did not yield with an easily identifiable yield point. The yield was assumed at 0.1% proof stress. A typical stress strain curve from the tensile machine is shown in Fig. 17. The results are given in the last row of Table 1 where it is seen that the tested mechanical properties fall some way short of the quoted properties. Further details can be found in Ref. [20].

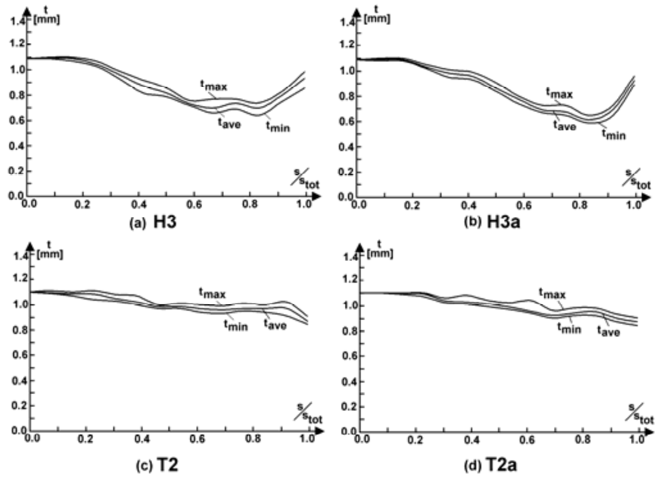

FIG. 19 Plot of average, maximum and minimum wall thickness versus meridional arc length (s ≡ apex). Results are shown for two nominally identical hemispheres H3/H3a and nominally identical pair of torispheres T2/T2a.

5.2 Manufacture, pre-test measurements and testing of domes

Domes were manufactured by spinning. Models were designed with a parallel length at the base as this allows for the dome to be attached to a base plate for testing. The parallel flange also serves to reduce any elastic 'spring-back' of the dome at the end of manufacture. The nominal dimensions of domes, comprising six hemispheres and four torispheres, is summarised in Table 3. The domes were spun against a mandrel of known dimensions, and as such all geometry is internal geometry. Photographs of two hemispheres and two torispheres are shown in Fig. 18 in as received state.
All the domes were measured for both shape and thickness. The density of measuring points corresponded to 10mm intervals along 16 meridians. It should be noted that domes H1 and H1a were measured on four meridians and at 5mm intervals due to their small size.

	ID (mm)	R_s/D	r/D (mm)	t (mm)	Parallel Flange Length (mm)
H1, H1a	89.0	---	---	1.1	20.00
H2, H2a	210.0	---	---	1.1	-
H3, H3a	145.0	---	---	1.1	-
T1, T1a	197.0	1.025	0.112	1.1	10.00
T2, T2a	150.0	0.80	0.167	1.1	10.00

TAB 3. Nominal dimensions of test domes. Note R_s and r are internal radii, measured from dimensions of manufacturer's spinning tool

The results of the thickness measurements showed that all of the domes had a good degree of axisymmetry. However, as expected, the thickness was non uniform along the meridian, and all the domes show thinning of the shell wall near the base. At latitudes corresponding to each measuring point the maximum, minimum, and average thicknesses have been plotted, and typical

	t_{min} (mm)	t_{max} (mm)	t_{ave} (mm)	St. dev (mm)
H1	0.630	1.245	0.945	0.151
H1a	0.745	1.220	0.965	0.128
H2	0.830	1.140	0.969	0.090
H2a	0.760	1.140	0.953	0.103
H3	0.640	1.100	0.891	0.151
H3a	0.590	1.100	0.883	0.170
T1	0.570	1.130	0.988	0.133
T1a	0.640	1.150	1.000	0.116
T2	0.840	1.110	1.007	0.068
T2a	0.840	1.100	0.999	0.078

TAB 4. Measured maximum, average, and minimum thicknesses of test domes.

distribution of wall thickness is plotted in Fig. 19. The pair of domes with the most uniform thickness distribution is T2 and T2a. For benchmarking purposes the maximum, minimum, average thicknesses and standard deviations of the domes have been listed in Table 4. X – Z coordinates of the outside surface of the domes were also measured. Using the measured coordinates, radii of best fit of the outside surface were calculated and they are provided in Table 5.

	ID (mm)	R_s (mm)	r (mm)	Parallel Flange Length (mm)
H1	86.58	41.82	---	20.00
H1a	86.63	41.57	---	20.00
H2	212.48	107.66	---	-
H2a	212.06	106.09	---	-
H3	151.87	75.85	---	-
H3a	151.73	76.51	---	-
T1	211.42	173.84	30.16	10.00
T1a	211.72	176.18	27.39	10.00
T2	148.10	124.15	27.55	10.00
T2a	147.96	125.47	26.25	10.00

TAB 5. Measured dimensions of test domes. Note R_s and r are measured best fit external radii.

The spun domes were affixed to a thick baseplate by machining a groove in the baseplate and using Wood's Metal to secure the dome in the groove. Domes which did not have a parallel flange had to be built in over a small portion of the shell wall, meaning that the hemisphere was reduced to a deep spherical cap. All domes were tested in a 350 mm dia x 1 m long pressure vessel located at Mechanical Engineering, The University of Liverpool. A single incremental pressure path was applied to all domes. The change in internal volume of the domes during pressurisation was recorded by measuring the mass of oil escaping from the inside of the domes.
All of the domes failed by a sudden loss in load carrying capacity, accompanied by a sudden outflow of oil during the test. The pressure to cause failure of the domes are listed in Table 6 where it is seen that the pairs of domes: (H1, H1a), (H2, H2a), (T1, T1a), (T2, T2a) show reasonable repeatability. Domes H3 and H3a, on the other hand, show some discrepancy in failure pressure. The ratio of H3/H3a is 5.93/4.83 = 1.23.
Dome H1 failed on the side, near the base, and dome H1a failing in an axisymmetric manner, at the apex of the

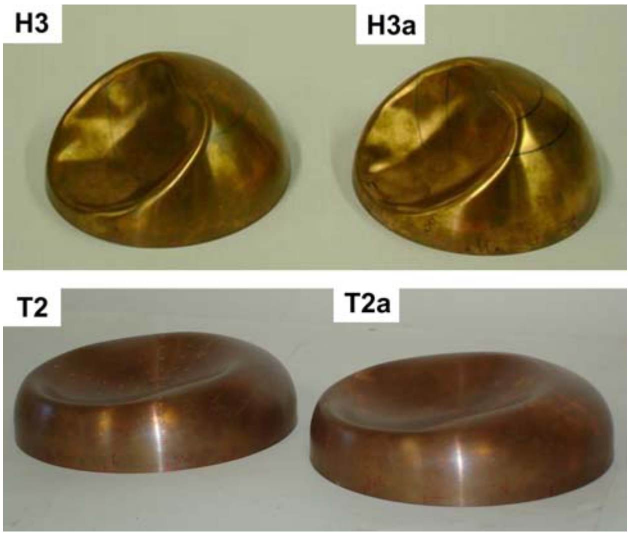

FIG. 20 View of collapsed hemispheres, H3/H3a and of two collapsed torispheres, T2/T2a.

dome. Similar behaviour was seen for H2 and H2a. Dome H2 failed at the top, H2a failed on the side of the dome. The failure modes of the remaining three pairs of domes were in agreement, i.e., both displaying a single inwards 'lobe' or dent. This demonstrates repeatability of the experiment in terms of failure mode for these cases. A sample of photographs of the domes after tests is shown in Fig. 20.

5.3 FE analysis – numerical analysis of measured geometries

The geometry and thicknesses of the FE models was based on measured data. There was some uncertainty over the material properties to use, and as such, three sets were chosen. The first two corresponded to: nominal upper and lower bounds on material properties, as quoted by the laminate manufacturer. The third set of material properties corresponded to the tested material properties, which were established previously (see last row in Table 1).
For the BOSOR5 analyses, best fit radii based on measured coordinates were used to model the meridian. The depth of the groove in the baseplate was taken into account, i.e., occupying a portion of the shell wall near the base. The shell wall thickness of the domes was modelled using a variable wall thickness profile, based on the hoop averaged thickness data as illustrated in Fig. 19.
For ABAQUS analyses the procedure was to create a 3D dome by revolving the best fit radius around the axis of revolution. As was for the BOSOR5 analyses, the radius was reduced from outside surface to mid-surface, by subtracting half average thickness. The thickness of the 3D dome was modelled by inputting individual nodal thicknesses into the model. A bi-cubic spline was used here to interpolate the nodal thicknesses between measured data points.
Failure of domes was first computed by BOSOR5. Failure of the domes was either by axisymmetric collapse, or bifurcation buckling occurring at the base of the dome. It is seen in Table 6 that the predictions based on the set of tested material properties fall some way short of the

		Lower		Higher		Tested	
	p_{exptl} (MPa)	p_{cr} (MPa)	p_{cr}/p_{exptl}	p_{cr} (MPa)	p_{cr}/p_{exptl}	p_{cr} (MPa)	p_{cr}/p_{exptl}
H1	9.46	9.43[c]	1.00	9.65[c]	1.02	7.18[c]	0.76
H1a	10.34	10.29[c]	0.99	10.78[c]	1.04	8.63[c]	0.83
H2	3.72	4.69[15]	1.26	5.33[11]	1.43	3.67[c]	0.99
H2a	3.62	4.49[15]	1.24	5.08[12]	1.40	3.35[14]	0.93
H3	5.93	5.53[c]	0.93	5.66[c]	0.95	4.28[c]	0.72
H3a	4.83	4.79[10]	0.99	4.90[10]	1.01	3.71[10]	0.77
T1	1.76	1.73[c]	0.99	1.98[c]	1.13	1.23[c]	0.70
T1a	1.71	1.63[c]	0.95	1.84[c]	1.07	1.18[c]	0.69
T2	3.07	3.21[c]	1.05	3.29[c]	1.07	2.44[c]	0.79
T2a	2.91	3.00[c]	1.03	3.09[c]	1.06	2.34[c]	0.80

TAB 6. Comparison of experimental results with BOSOR5 predictions.

experimental collapse pressures (except for H2 and H2a). Predictions based on the nominal/quoted material properties were in better agreement with experimental results. Thus it was decided to use the nominal/quoted material properties for 3D ABAQUS analyses.

		Lower		Higher	
	p_{exptl} (MPa)	p_{cr} (MPa)	p_{cr}/p_{exptl}	p_{cr} (MPa)	p_{cr}/p_{exptl}
H1	9.46	9.75[c]	1.03	9.95[c]	1.05
H1a	10.34	10.83[c]	1.05	10.98[c]	1.06
H2	3.72	4.84[0]	1.30	4.92[c]	1.32
H2a	3.62	4.51[0]	1.25	4.59[c]	1.27
H3	5.93	5.53[c]	0.93	5.63[c]	0.95
H3a	4.83	4.91[c]	1.02	4.93[c]	1.02
T1	1.76	1.53[c]	0.87	1.58[c]	0.90
T1a	1.71	1.42[c]	0.83	1.46[c]	0.86
T2	3.07	3.07[c]	1.00	3.15[c]	1.03
T2a	2.91	3.03[c]	1.04	3.08[c]	1.06

TAB 7. Comparison of experimental results with ABAQUS predictions.

The results of the ABAQUS 3D analyses are summarised in Table 7 where it is seen that there is reasonable agreement for all domes except H2 and H2a which both failed experimentally at lower pressures than were predicted by ABAQUS. Fig. 21a show domes H3 and H3a both failed by local collapse, occurring near the base of the dome. For torispherical domes, collapse took place at the junction between knuckle and crown (see Fig. 21b).

6. COMPARISON OF RESULTS

Comparing the results from the BOSOR5 axisymmetric analysis reveals that the analysis accurately predicts the failure pressure of the domes, with the exception of the hemispheres H2 and H2a. Using the lower of the mechanical properties stated by manufacturer produced the most accurate results.

As with the BOSOR5 analysis, the ABAQUS analyses predicted the failure pressure of the domes with a reasonable level of success. With the exception of H2 and H2a, the accuracy of the results from ABAQUS range from -17% to +3% (with the negative value indicating a numerical underestimation of failure pressure, i.e. safer scenario). For domes H2 and H2a the BOSOR5 analysis differs from the experimental results by +26% and +24% and the ABAQUS differs by +30% and +25%. Although there is a larger discrepancy between the experimental and numerical results, both analyses are comparable with each other.

The discrepancies between the numerical analyses and the experimental results can be attributed to imperfections, in particular at the apex of the domes. The domes were spun with holes at the top, which were plugged with a nut, bolt, and washer. The torque applied to the nut and bolt would induce some residual stress at the top of the domes which may have caused the domes to fail at a lower pressure. Furthermore, the domes were spun without a parallel flange at the base. As such, there would have been a larger degree of elastic ‘spring-back’ in H2 and H2a, and as such a deviation from perfectly hemispherical meridian.

7. POST TEST ANALYSIS OF HYBRID MATERIAL

To gain more insight, it was decided to analyse the material from which they had been constructed. The aim was to cut several coupons from the domes and analyse the hybrid laminate under an optical microscope. This would allow a check for signs of delamination after testing to be made, and also to measure the thicknesses of the individual layers of the hybrid sheet. Three coupons were cut from domes H2 and T2 after testing. One coupon was taken from the damaged area of the dome, one from the non-damaged area, and a third from the junction between damaged and non-damaged areas (region of highest deformation).

The coupons were prepared in a resin mould and then polished on rotating tables using paper of grades 60 – 2500. A one micron finish was then achieved using a rotating table and oil.

The specimens were photographed under magnification of 20x and 100x. Fig. 22a shows coupon from region of highest deformation at magnification of 20x. The calibrated scale bar is in units microns, i.e., 1000 on the scale bar = 1mm. It is seen that the coupon is just over 1.1mm in thickness. This corroborates with earlier thickness measurements of the shell. Fig. 22b shows coupon the same coupon at magnification of 100x. The calibrated scale bar is also in units of microns and it is seen that the

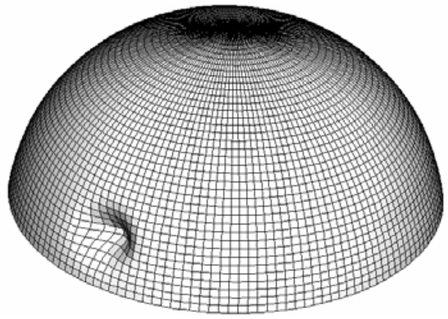

H3

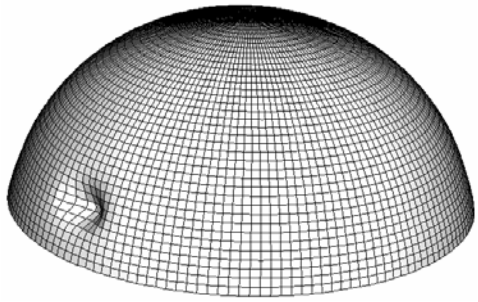

H3a

FIG. 21a Post-collapse deformation of hemispheres H3 and H3a.

copper layer is approximately 50 microns in thickness. This corroborates with the value quoted by the manufacturer.

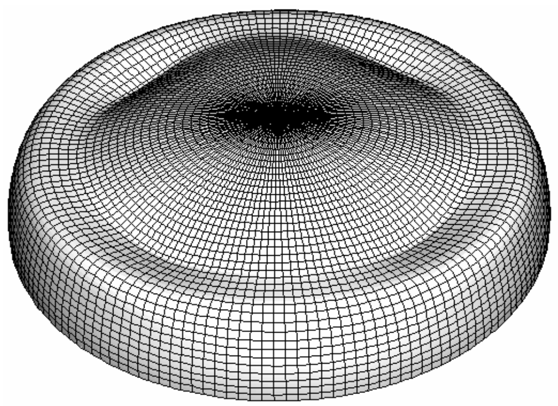

T2

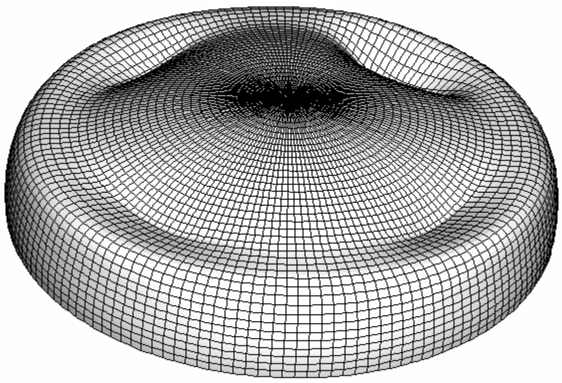

T2a

FIG. 21b Post-collapse deformation of torispheres T2 and T2a.

From Fig. 22 it is seen that there are no visible signs of delamination in any of the coupons, however there are several visible inclusions between the copper and steel, these may be due to oil or grit from the paper of the rotating tables used to polish the coupon.

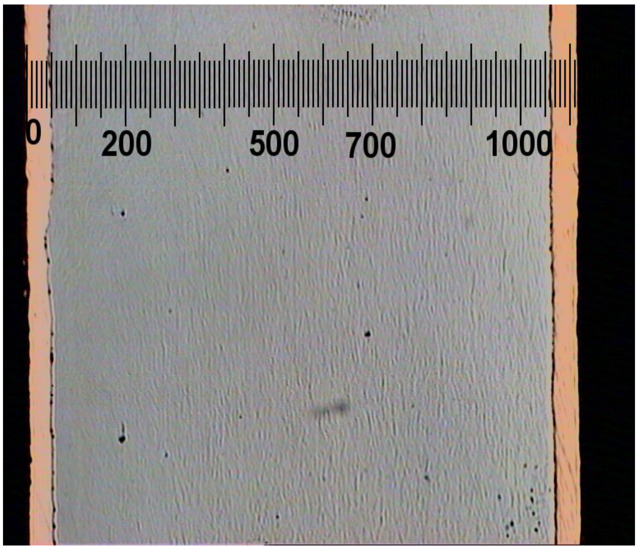

(a)

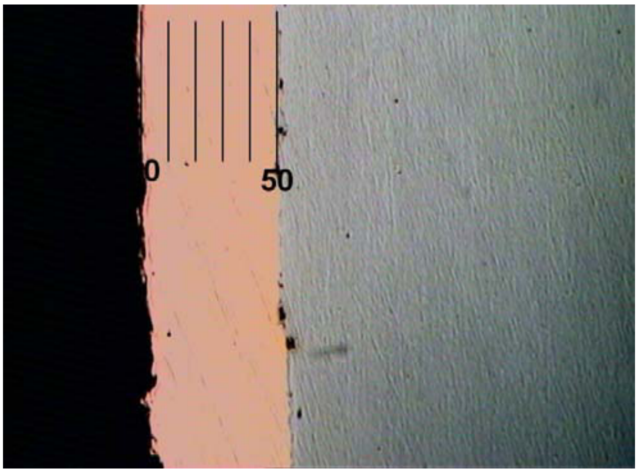

(b)

FIG. 22 Photographs through cross section of copper-steel-copper hybrid sheet. (a) Magnification = 20x. (b) Magnification=100x.

8. CONCLUSIONS

This paper has, through experiment and numerical calculations (both axisymmetric and 3D), revealed a number of difficulties which exist when dealing with layered metallic shells. These include: establishing a comprehensive set of material data for the laminate, and dealing with apex boundary conditions.

As there is no other available experimental data in the literature it is difficult to generalise the findings of the paper. However, the following observations can be made:

- It is possible to achieve a required pressure resistance with several combinations of layer thicknesses and materials, giving designers a choice dependant on cost manufacturability, etc.
- When supported by a steel core, copper outer layers are,

at buckling, nearly entirely plastically strained due to the effects of external pressure.

9. REFERENCES

[1] S.E. Rutgerson, W.J. Botega, “Thermo-elastic buckling of layered shell segments”, Intl J. Solids and Structures, vol. 39, 2002, 4867-4887.
[2] M. Batista, F. Kosel, “Thermoelastic stability of double-layered spherical shell”, Intl J. of Non-linear Mechanics, vol. 41, 2006, 1016-1027.
[3] Guz A.N. Dyshel M.Sh., “Buckling and cracking characteristics of two-layered plate in tension”, Theoretical and Applied Fracture Mechanics, vol. 38, 2002, 103-107.
[4] N.F. Kazakov, A.V. Sergeev, N.I. Stepanova, A.N. Kharitonova, “Evaluation of residual stresses in layered metal composites”, Strength of Materials, vol. 16, 1984, 399-402.
[5] J. Blachut, G.D. Galletly, D.N. Moreton, “Buckling o near-perfect steel torispherical and hemispherical shells subjected to external pressure”, AIAA J., vol. 28, 1990, 1971-1975.
[6] J.G. Teng, “Buckling of thin shells: recent advances and trends”, Applied Mechanics Reviews, Transactions of the ASME, vol. 49, 1996, 263-274.
[7] J. Blachut, “Pressure vessel components: some recent developments in strength and buckling”, Progress in Structural Eng. and Materials, vol. 1, no. 4, 1998, 415-421.
[8] J. Blachut, O.R. Jaiswal, “On the choice of initial geometric imperfections in externally pressurized shells”, J. Pressure Vessel Technology, Transactions of the ASME, vol. 121, 1999, 71 – 76.
[9] ASME B&PV Code, Section VIII, Division 2, 2004 Edition, New York, USA, ISBN 0791828921.
[10] BSI, “Published Document PD5500: Specification for Unfired Pressure Vessels”, 2003 BSI, London, ISBN 0580411265.
[11] European Convention for Constructional Steelwork Recommendations “Buckling of steel Shells – European Recommendations”, ECCs – TWG 8.4, Fourth Edition, 1988, Brussels, (under review).
[12] P. Smith, J. Blachut, “Buckling of externally pressurised prolate ellipsoidal domes”, J. Pressure Vessel Technology, Trans. of the ASME, 2007, (in print).
[13] J. Blachut, G.D. Galletly, “Clamped torispherical shells under external pressure – some new results”, J. of Strain Analysis, vol. 23, 1988, 9-24.
[14] J. Blachut, G.D. Galletly, A.G. Gibson, “CFRP domes subject to external pressure”, Marine Structures, vol. 3, 1990, 149-173.
[15] L. Dong, J. Blachut, “Analysis and collapse of thick composite torispheres”, Proc Instn Mech Engrs, vol. 212, Part E, 1998, 103-117.
[16] J. Blachut, “Influence of meridional shaping on the collapse strength of FRP domes”, Engineering Optimization, vol. 19, 1992, 65-80.
[17] H.D. Hibbitt, B.I. Karlsson, E.P. Sorenseen, “ABAQUS – Theory Manual”, Version 6.4, Pawtucket, RI, 028604847, USA.
[18] D. Bushnell, BOSOR5 – program for buckling of elasti-plastic complex shells of revolution including large deflections and creep”, Computers Structures, vol. 6, 1976, 221-239.
[19] BSI, BS EN 10002-1, London, 2001.
[20] P. Smith, “Optimisation of shell components subject to stability criteria”, PhD Thesis, The University of Liverpool, 2007.